Journal of Hazardous Materials 205–206 (2012) 229–235

Contents lists available at SciVerse ScienceDirect

Journal of Hazardous Materials

journal homepage: www.elsevier.com/locate/jhazmat

P25–graphene hydrogels: Room-temperature synthesis and application for removal of methylene blue from aqueous solution

Chengyi Hou[a,b], Qinghong Zhang[a], Yaogang Li[b,*], Hongzhi Wang[a,**]

[a] State Key Laboratory for Modification of Chemical Fibers and Polymer Materials, Donghua University, Shanghai 201620, PR China
[b] College of Materials Science and Engineering, Donghua University, Shanghai 201620, PR China

ARTICLE INFO

Article history:
Received 3 November 2011
Received in revised form 8 December 2011
Accepted 28 December 2011
Available online 10 January 2012

Keywords:
Graphene
Hydrogel
Titanium dioxide
Photocatalyst
Environmental protection

ABSTRACT

Herein we report a room-temperature synthesis of chemically bonded TiO_2 (P25)–graphene composite hydrogels and their use as high performance visible light photocatalysts. The three-dimensional (3D) TiO_2–carbon composite exhibits a significant enhancement in the reaction rate in the decontamination of methylene blue, compared to the bare P25. The 3D P25–graphene hydrogel is much easier to prepare and apply as a macroscopic device, compared to the 2D P25–graphene sheets. This work could provide new insights into the room-temperature synthesis of graphene-based materials. As a kind of the novel 3D graphene-based composite, the obtained high performance P25–graphene gel could be widely used in the environmental protection issues.

1. Introduction

Graphene is a two-dimensional (2D) structure of carbon atoms. Since it was isolated in 2004 [1], graphene has attracted great attention due to its extraordinary electrical, thermal, and mechanical properties [2–4]. These unique properties offer great promise for many practical applications such as energy-storage [5–7], composite reinforcement [8–10], and catalysis [11,12]. In general, graphene can be synthesized through several chemical methods such as chemical vapor deposition, epitaxial growth, and the creation of colloidal suspensions [13]. Recently, novel three-dimensional (3D) graphene-structured materials have been prepared through varied methods [14–21]. However, literature on the relatively low temperature (below 100 °C) synthesis of graphene materials is limited [17,18,20,21]. Particularly, room-temperature route to synthesize 2D graphene sheets is infrequent [21], not to mention the 3D graphene materials.

Graphene hydrogel, consist of 3D graphene networks, is electrically conductive, mechanically strong, and thermally stable [16–18]. As a new kind of 3D graphene materials and inorganic hydrogel materials, graphene hydrogel is attractive in the fields of biotechnology and electrochemistry. However, as mentioned above, the recent reported easy and green synthesis route of graphene hydrogels still needs heating reactions. Moreover, functionalization of the as-prepared graphene hydrogels is limited, as well.

As an important member of functionalized graphene materials, inorganic nanomaterial–graphene composite has myriad of potential applications [22]. In particular, P25–graphene composite is recently found to be a more efficient photocatalyst compared to P25 and P25–carbon nanotubes due to its giant 2D planar structure [23]. In this TiO_2–C composite, graphene could act as an acceptor for the photogenerated electrons from the UV light excited P25 and ensure fast charge transportation in view of its high conductive. Therefore, 3D TiO_2–graphene composite is expected to be an efficient photocatalyst. On the other hand, the integration of nanostructured materials into macroscopic devices that can translate phenomena at the nanoscale to the macroscopic level proves the key to paving the way to realizing applications of nanomaterials [24]. Therefore, Macroscopic 3D P25–graphene materials such as P25–graphene hydrogels deserve special attention owing to their macroscopic scale and the more practical use as available devices, compared to 2D P25–graphene sheets. Unfortunately, in addition to TiO_2-based 3D TiO_2–graphene composite [25], graphene-based 3D TiO_2–C composite has not been reported yet.

Herein, we demonstrate a room-temperature route to obtain self-assembled graphene hydrogels as well as functionalized composite hydrogels by incorporation of multi-walled carbon nanotubes (MWCNTs) or P25 nanoparticles. The formation mechanisms for the graphene-based composite hydrogels are studied. The photocatalytic properties of P25–graphene hydrogels and their use as environmental remediation devices are investigated.

* Corresponding author. Tel.: +86 21 67792676; fax: +86 21 67792855.
** Corresponding author. Tel.: +86 21 67792881; fax: +86 21 67792855.
E-mail addresses: yaogang_li@dhu.edu.cn (Y. Li), wanghz@dhu.edu.cn (H. Wang).

0304-3894/$ – see front matter © 2012 Published by Elsevier B.V.
doi:10.1016/j.jhazmat.2011.12.071

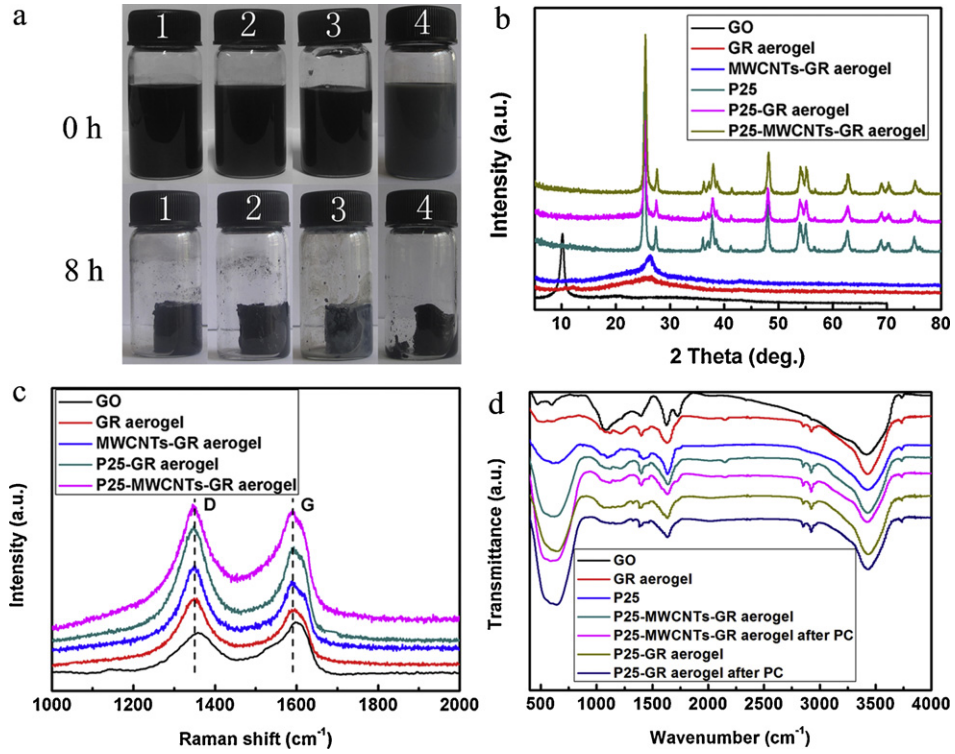

Fig. 1. a: Photographs of initial solutions (0 h) containing GO (1), MWCNTs and GO (2), MWCNTs, P25, and GO (3), P25 and GO (4), respectively and the obtained hydrogels after the 8 h room-temperature reaction; b: XRD patterns of GO, P25, and the as-prepared samples; c: Raman spectra of GO and the as-prepared samples; d: FTIR spectra of GO, P25, and the as-prepared samples. GR stands for graphene and PC stands for photocatalysis.

2. Experimental

2.1. Reagents

Natural flake graphite powder (99.95%, 500 mesh) was purchased from YiFan Ltd. Co. (Shanghai, China), MWCNTs with length 5 μm, o.d. 30–90 nm, and MWCNT content >95%, were purchased from Shenzhen Nanotech Port Ltd. Co., P25 TiO_2 nanopowders (Degussa P25 grade, 20% rutile and 80% anatase, with a specific surface area of 50 $m^2\ g^{-1}$) were purchased from Degussa. All other reagents were purchased from Sinopharm Chemical Reagent Ltd. Co. All reagents were of analytical grade and used as obtained without further purification.

2.2. Synthesis of graphite oxide (GO)

GO was prepared using Hummers' method [26] and described in brief as follows: 3 g natural flake graphite powder was added to 69 mL cold (0 °C) concentrated H_2SO_4. 9 g $KMnO_4$ was then added gradually with stirring and cooling in an ice bath. The mixture was then stirred at 35 °C for 2 h. 138 mL distilled water was slowly added to the mixture and the temperature of the mixture was maintained below 100 °C for 15 min. After that, 420 mL 30% H_2O_2 solution was added to the mixture. Finally, the mixture was washed with 750 mL 10% HCl aqueous solution to remove metal ions and then thoroughly washed with distilled water. The final solution was concentrated to 4 mg mL^{-1}.

2.3. Synthesis of graphene hydrogels

In a typical procedure, 0.24 g L-ascorbic acid and 0.25 mL hydrazine hydrate were dispersed to 20 mL 4 mg mL^{-1} GO aqueous solution by ultrasonication for 30 min. The mixture was put at room-temperature (25 °C) for about 8 h. Then the reduced graphite oxide hydrogels were immersed in water to remove impurities and cleaned for further investigation.

Composite hydrogels were obtained follow the same procedure, 0.24 g L-ascorbic acid, 0.25 mL hydrazine hydrate, 200 mg P25 were dispersed to 20 mL 4 mg mL^{-1} GO aqueous solution by ultrasonication for 30 min, P25–graphene hydrogels were obtained at room-temperature after about 8 h; 0.24 g L-ascorbic acid, 0.25 mL hydrazine hydrate, 40 mg MWCNTs were dispersed to 20 mL 2 mg mL^{-1} GO aqueous solution by ultrasonication for 30 min, MWCNTs-graphene hydrogels were obtained at room-temperature after about 8 h; 0.24 g L-ascorbic acid, 0.25 mL hydrazine hydrate, 200 mg P25, 40 mg MWCNTs were dispersed to 20 mL 2 mg mL^{-1} GO aqueous solution by ultrasonication for 30 min, P25-MWCNTs-graphene hydrogels were obtained at room-temperature after about 8 h.

All hydrogels were freeze-dried for characterization and photocatalytic experiments.

2.4. Photocatalytic experiments

The photodegradation of methylene blue (MB) dyes was observed based on the absorption spectroscopic technique. In a typical process, aqueous solution of the MB dyes (0.01 g L^{-1}, 40 mL) and the photocatalysts (P25, P25-MWCNTs-graphene, and P25–graphene, 30 mg) were placed in a cylindrical quartz vessel. Under room conditions and stirring, the vessel was exposed to the UV irradiation produced by a 300 W high pressure Hg lamp (the average light intensity was 30 mW cm^{-2}) with the main peak at wavelength of 365 nm. All other lights were insulated. At given time intervals, the photoreacted solution was analyzed by recording the maximum absorbance of MB at 660 nm with the UV–vis spectrophotometer (PerkinElmer Lambda-35).

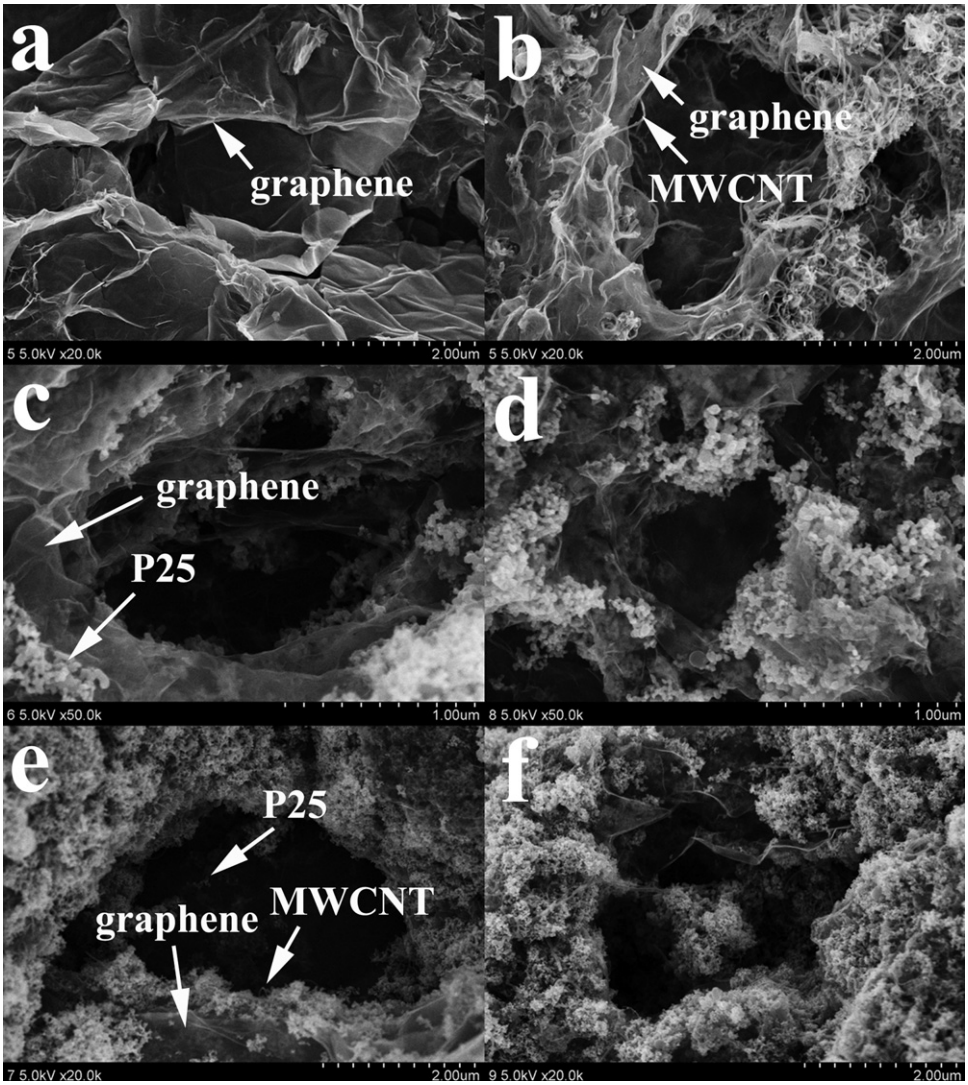

Fig. 2. FESEM images of the graphene-based aerogel. a: graphene gel; b: MWCNTs-graphene gel; c: P25–graphene gel; d: P25–graphene gel after photocatalysis; e: P25-MWCNTs-graphene gel; f: P25-MWCNTs-graphene gel after photocatalysis.

Mixture underwent four consecutive cycles. Dark adsorption experiments were carried out too. In the visible light photocatalysis, a similar procedure was constructed with a 500 W xenon lamp equipped (the average light intensity was 55 mW cm^{-2}) with a 420 nm cutoff filter [27].

2.5. Characterization

Fourier transform infrared (FTIR) spectra were recorded on a Nicolet NEXUS-670 spectrometer with KBr pellets in the 4000–800 cm^{-1} region.

Powder X-ray diffraction (XRD) spectroscopy was carried out on a Rigaku D/max 2550 V X-ray diffractometer using Cu K_α irradiation (λ = 1.5406 Å). The operating voltage and current were kept at 40 kV and 300 mA, respectively.

The morphology of the as-prepared products was determined at 20 kV by a JSM-6700F field emission scanning electron microscopy (FESEM).

Raman spectra were recorded on a Renishaw in plus laser Raman spectrometer with λ_{exc} = 785 nm.

Diffuse reflectance spectra (DRS) were recorded in the range from 250 to 800 nm using the UV–vis spectrophotometer (PerkinElmer Lambda-950).

Specific surface areas of the catalysts were measured at 77 K by Brunauer–Emmett–Teller (BET) nitrogen adsorption–desorption (Quantachrome Instruments, USA).

3. Results and discussion

Graphene-based hydrogels were prepared by reduction of GO in aqueous solutions. As shown in Fig. 1a, well-formed hydrogels self-assembled from initial solutions containing GO, MWCNTs, or P25. Through co-reducing effect of L-ascorbic acid and hydrazine hydrate, room-temperature synthesis and functionalization of graphene hydrogels is realized. L-ascorbic acid helps to form uniform aquatic gels, during which procedure gradually restored strong π–π interaction among the reduced graphite oxide sheets is the main reason for the gelation [17,18]. The no-heating gelation reaction and the fast gelation speed could be attributed to the strong reducing effect of hydrazine hydrate. The obtained hydrogels were freeze-dried to aerogels for further characterizations.

Fig. 1b shows the XRD patterns of GO, P25, and the as-prepared samples. In all graphene-based gel samples, (0 0 1) reflection peak of GO at around 2θ = 10.8° disappeared and new peaks are observed at around 2θ = 25.9° and 26.5° in graphene and MWCNTs-graphene samples respectively, corresponding to carbon species.

The results indicate the high-effective reduction of GO. In addition, P25–graphene and P25-MWCNTs-graphene show similar XRD pattern with pure P25, and no diffraction peak for carbon species is observed in these composites, which is due to the low amount and relatively low diffraction intensity of graphene and MWCNTs.

The reduced mechanism of GO to reduced graphene sheets in graphene-based composite gels was also studied through the Raman spectrum. In Fig. 1c, all spectra show the existence of the G band and D band, which are E_{2g} vibrational mode in plane and A_{1g} breathing mode, respectively. The intensity ration of the D and G band (I_D/I_G) changes from 0.78 (GO) to around 1.17 (graphene-based gels), indicating a decrease in the average size of the sp^2 domains upon the reduction of GO.

Fig. 1d shows the FTIR spectra of GO, P25, and the as-prepared samples. In GO spectrum, the C=O stretching of COOH groups sat at edges of GO sheets is observed at 1725 cm^{-1}. The absorptions due to the O—H bending vibration, epoxide groups and skeletal ring vibrations are observed around 1635 cm^{-1}. The absorption at 1400 cm^{-1} may be attributed to tertiary C—OH groups [28]. For graphene-based gels, the absorption due the C=O group (1725 cm^{-1}) is decreased obviously in intensity and absorptions at 1635 and 1400 cm^{-1} are absent, indicating the reduction of GO. Moreover, the chemical bonding between P25 and graphene in the composite gels could be deduced. Pure P25 show a low frequency band around 588 cm^{-1}, which corresponded to the vibration of Ti—O—Ti bonds. In contrast, in the as-prepared P25–graphene composite, a much plumper absorption is observed at around 642 cm^{-1}, which could be attributed to a combination of Ti—O—Ti vibration and Ti—O—C vibration [29]. The presence of Ti—O—C bonds indicates the formation of chemically bonded P25–graphene composites [23]. However, in the P25-MWCNTs-graphene composite, the plumper peak shifts back to low wavenumber (599 cm^{-1}), indicating the absence of Ti—O—C bonds, which could be due to the strong π–π conjugation between the reduced graphite oxide and MWCNTs, as a result of which MWCNTs might adsorb on the reduced graphite oxide sheets preferentially during the gelation procedure and P25 combined with MWCNTs through physical adsorption subsequently. This could be confirmed and demonstrated by FESEM analyses and diagrammatic sketches as follows.

Fig. 2 shows the FESEM images of the freeze-dried graphene-based hydrogels. The well-defined and interconnected 3D porous network of the resulting gels is revealed in these images. The microstructure of the graphene-based composite samples is similar to the pure graphene sample. The pore sizes of the network are in the range of submicrometer to several micrometers and the walls consist of thin layers of stacked graphene sheets. As shown in Fig. 2b and c, MWCNTs and P25 dispersed on the graphene support and can be observed on both outer and inner walls of the porous. As discussed above, they are chemically combined with graphene sheets in MWCNTs-graphene and P25–graphene composites, respectively. In P25-MWCNTs-graphene samples, MWCNTs are densely covered with P25 nanoparticles and barely no individual P25 is observed on the graphene support (see Fig. 2e and SupplementaryFigure S1), indicating the unsuccessful formation of chemical bonds between P25 and graphene sheets, which is in accord with the FTIR results.

The diagrammatic sketches of the formation for different graphene-based composite hydrogels are demonstrated in Fig. 3. With the reduction proceeding, the π-conjugated structures of reduced GO sheets are increased which increases the amount of π–π stacking cross-links between graphene sheets. The partial overlapping or coalescing of flexible graphene sheets results in construction of the 3D structures. The residual oxygenated functional groups on the graphene sheets (see SupplementaryFigure S2) could entrap ample water into the graphene network to form graphene-based hydrogels. In P25–graphene hydrogels,

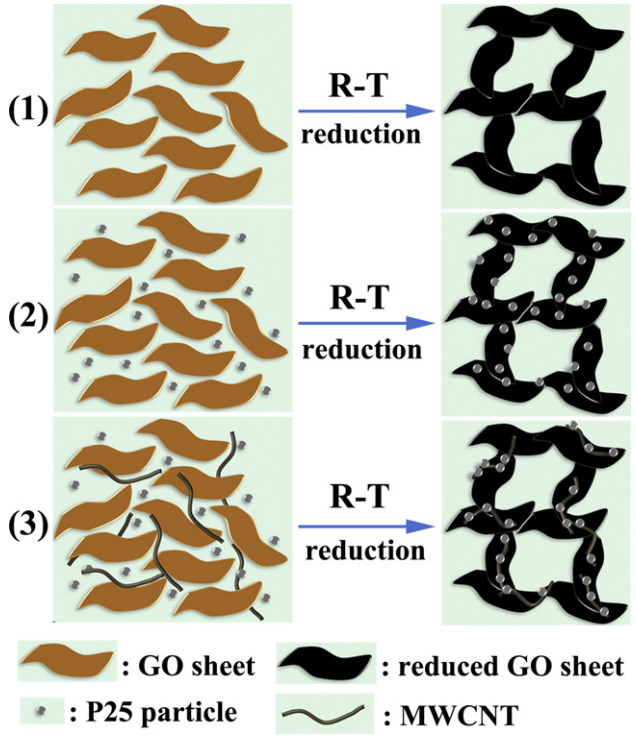

Fig. 3. The diagrammatic sketches of the formation for graphene hydrogels (1), P25–graphene hydrogels (2), and P25-MWCNTs-graphene hydrogels (3). R-T stands for room-temperature.

Ti—O—C bonds are formed between P25 nanoparticles and graphene sheets. In P25-MWCNTs-graphene hydrogels, P25 are adsorbed on MWCNTs, which interferes connections between P25 and graphene. The difference between P25–graphene and P25-MWCNTs-graphene hydrogels is the presence or absence of chemical bonds between nanoparticles and graphene sheets. In chemically bonded TiO_2–graphene composite sheets, graphene could act as an acceptor of the photogenerated electrons by TiO_2 and ensure fast charge transportation (to suppress charge recombination) in view of its high conductivity, leading to an enhancement in the photocatalytic performance [23]. Therefore, it is expected that our 3D P25–graphene composites could act as a more efficient photocatalyst compared to the bare P25 and 3D P25-MWCNTs-graphene hydrogels. In addition, electrons could transfer stereoscopically in P25–graphene hydrogels through the 3D graphene networks whereas they would be confined to a plane in 2D P25–graphene sheets, as shown in Fig. 4. The advantage of 3D networks in P25–graphene hydrogels makes them much more attractive as macroscopic devices.

The photocatalytic activities of P25 powders, dried P25–graphene, and P25-MWCNTs-graphene gels were measured by the decontamination of MB as model reaction under

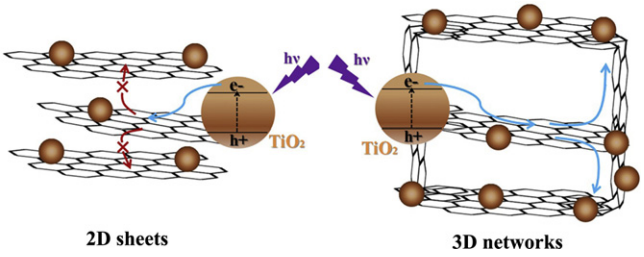

Fig. 4. Schematic diagrams for illuminating the charge behavior at interfaces in 2D P25–graphene sheets and 3D P25–graphene networks.

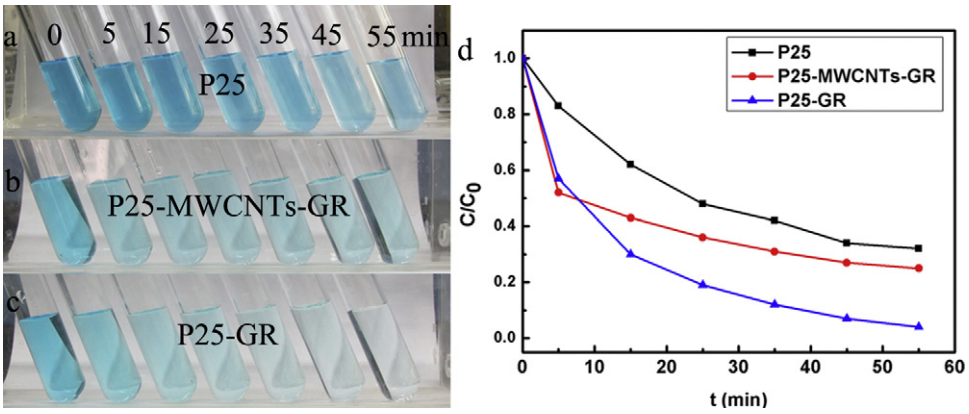

Fig. 5. Photodegradation of MB under UV light irradiation. a–c: Photographs of MB solutions with different photocatalyst at a given time interval; d: the corresponding concentration changes of MB during the photodegradation.

UV light. Under irradiation, the P25 were excited and the photogenerated carriers could transfer to the nearby MB and take part in the redox reactions, leading to the decomposition of MB into CO_2 and H_2O [30]. The normalized temporal concentration changes (C/C_0) of MB during the decontamination were derived from the changes in the dye's absorption profile ($\lambda = 660$ nm) at a given time interval. As shown in Fig. 5a–c, the MB solution containing P25-graphene photocatalysts fades with time observably, whereas the decontamination effects are weak in other groups. The corresponding concentration changes of MB are shown in Fig. 5d. It is clear that the P25–graphene sample shows significant progress in the decontamination of MB compared to pure P25 and P25-MWCNTs-graphene. Under UV light irradiation, about 96% of the initial dyes were decomposed by P25–graphene after less than 1 h. In contrast, nearly 32 and 27% of the initial dyes still remained in the solution after the same time period for pure P25 and P25-MWCNTs-graphene, respectively. Moreover, by extending the time of decontamination reactions, it was found that it needs more than 3 h to completely decompose dyes using P25 and P25-MWCNTs-graphene, and for P25–graphene, it just takes about 1 h. In addition, the durability of the high performance 3D P25-graphene catalyst was also checked. The decontamination of MB was monitored for four cycles and there was no significant decrease in decontamination rate during this process (see SupplementaryFigure S3). The catalysts were collected, washed, dried and re-characterized after the experiments. In FTIR spectra and FESEM images, no significant changes are observed in the second-freeze-dried samples and it is worth mentioning that the obtained P25–graphene and P25-MWCNTs-graphene composites maintained their 3D microstructures, indicating both the good chemical and physical stability of the 3D graphene-based composite materials.

In addition to the effect of suppressed charge recombination by graphene, another factor that plays important roles during the photocatalysis is the adsorptivity of the TiO_2-graphene catalyst. Compared to P25 and P25–carbon nanotubes composites, the enhanced adsorptivity of the traditional 2D P25–graphene composite sheets could be mainly attributed to its giant π-conjugation system and 2D planar structure [23]. Our novel 3D P25–graphene composite are therefore more attractive due to its 3D porous stereostructure. As shown in Fig. 6, the adsorption of MB dyes on pure P25 in the dark is negligible after 10 min and the MB removal is only 8%. In contrast, The MB removal is 38% and 78% for P25-MWCNTs-graphene and P25–graphene sample respectively at equilibrium after about 50 min. The results indicate that the adsorptivity of P25–graphene is much stronger than that of P25-MWCNTs-graphene, which might be attributed to the stronger adsorptivity of graphene compared to MWCNTs. The effect of 3D graphene and MWCNTs-graphene products without P25 for adsorption was also investigated (see SupplementaryFigure S4), the stronger adsorption of MB in dark on graphene than that on MWCNTs-graphene supports the previous result that the adsorptivity of graphene plays important roles during the decontamination of MB. It is worth mentioning that there are no significant changes in the BET specific area of the 3D P25–graphene composites (47 $m^2\,g^{-1}$) compared to P25 powders (50 $m^2\,g^{-1}$), indicating that the enhanced adsorptivity of the P25–graphene composite could be mainly attributed to its 3D porous stereostructure.

As mentioned above, the advancement of the P25–graphene in the photocatalysis can be partly attributed to the enhanced adsorptivity. However, adsorption is not the only influential factor. The physical mixture of P25 and dried graphene gels showed much poorer activity in the photodegradation compared to our chemically bonded P25–graphene composites (see SupplementaryFigure S5). Accordingly, the chemical bonds between P25 and graphene contribute effectively to the enhanced photoactivity. Furthermore, our 3D chemically bonded P25–graphene composites show a faster decontamination rate (~96% of the initial dyes were decomposed in 55 min), compared to the 2D chemically bonded P25–graphene sheets (~85% of the initial dyes were decomposed in 55 min) under the same experimental condition [23]. Considering that there are no significant changes in the BET specific area of the 3D P25–graphene composites (47 $m^2\,g^{-1}$) compared to the 2D P25–graphene sheets (51 $m^2\,g^{-1}$), the enhanced decontamination rate of our products could be mainly attributed to the 3D graphene networks, which is

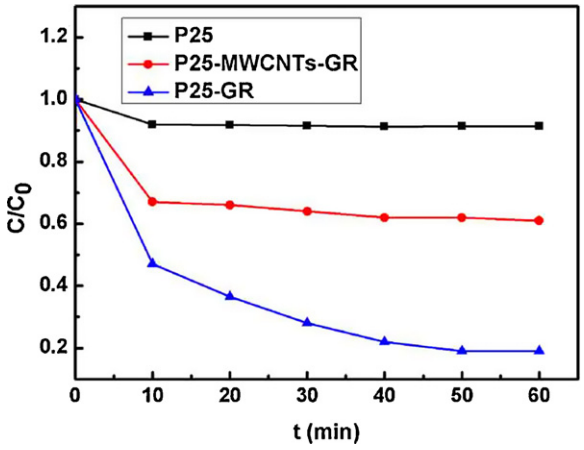

Fig. 6. Adsorption of MB in dark on different photocatalyst.

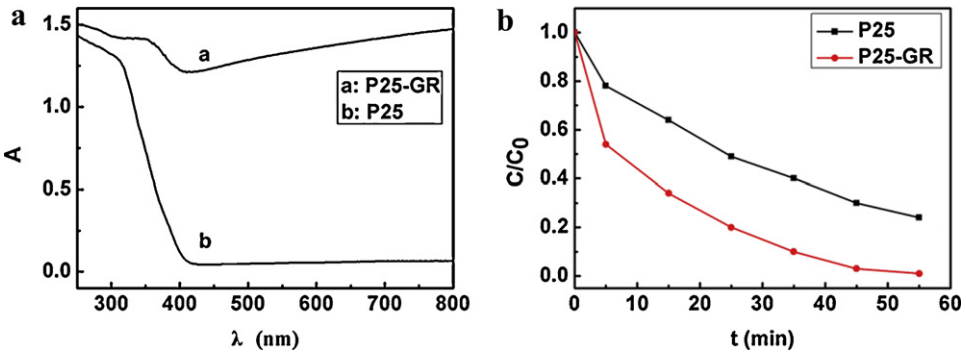

Fig. 7. a: Diffuse reflectance spectra of different catalysts; b: photodegradation of MB under visible light irradiation over different catalysts.

an advanced structure that contributes to photocatalytic properties as illuminated in Fig. 4.

In addition, carbon species might strongly affect the light absorption range of photocatalysts, which plays an important role in the photocatalysis, especially for the visible light photocatalysis. As shown in Fig. 7a, significant enhance in absorption intensity can be observed in P25–graphene samples, especially in the range of visible light. Moreover, there is an obvious red shift in the absorption edge from 385 to 405 nm of P25–graphene sample, compared to P25. The result indicates the narrowing of the band gap of P25 triggered by chemical bonding between P25 and graphene, according with the FTIR and FESEM results. For P25–graphene composites, the energy band gap of about 3.06 eV is lower than that of the standard commercial P25 employed in this study (3.22 eV), indicating that in the as-prepared composites the photoactive TiO_2 is able to absorb photons not only from UV irradiation but also visible light [31]. The extended light absorption range makes the P25–graphene composites good candidates for visible light photocatalysis. Fig. 7b demonstrates the visible light photodegradation of MB using P25 and P25-graphene as photocatalysts. It is clear that the P25–graphene sample shows significant progress in the photodegradation of MB compared to pure P25. Under visible light irradiation, the initial dyes were completely decomposed by P25–graphene after less than 1 h. In contrast, nearly 24% of the initial dyes still remained in the solution after the same time period for pure P25.

The outstanding UV and visible light photoactivities of the 3D P25-graphene catalyst is expected to facilitate its use in practical environmental remediation. In contrast with 2D P25–graphene sheets, the graphene hydrogel is an available device itself. As shown in Fig. 8a, it could be *in situ* synthesized in a quartz tube and effectively clean the MB solution flow (10 mg L^{-1}, inset 1). The filtrate (inset 2) is almost clear. This result could be attributed to

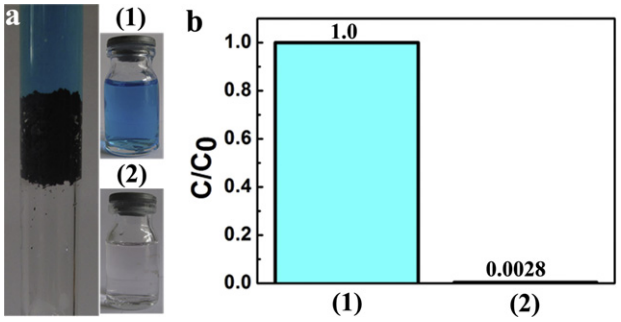

Fig. 8. a: Photographs of the P25-hydrogel device and the MB solutions before and after filtering through this device (inset 1 and 2); b: bar plot showing the MB concentration in solutions. C_0 is the concentration of 10 mg L^{-1} MB solution.

the strong adsorptivity of the 3D P25-graphene catalyst as discussed before. MB concentration in the clean solution is calculated to be 0.028 mg L^{-1} (see Fig. 8b) that could be ignored in this experiment. To investigate the maximum adsorption capacity of MB to the P25–graphene hydrogels, concentrated MB solution (100 mg L^{-1}) are filtered through the hydrogel (1.8 cm^3, aspect ratio: 1.9:1.1) with a flow rate of 5 mL min^{-1}. The maximum adsorption capacity (q) of MB to the hydrogel is calculated from the concentration difference of the solution at the beginning and at equilibrium according to the equation:

$$q = \frac{(C_0 - C_e)V}{m} \quad (1)$$

where C_0 and C_e are the initial and equilibrium concentration of MB (mg L^{-1}), respectively. V is the volume of the solution (mL) and m is the amount of P25–graphene (g). The value is obtained as much as 87.63 mg g^{-1}. In addition, the MB dyes adsorbed on P25–graphene hydrogels could be easily photodegraded by P25–graphene under UV or visible light irradiation. The device we described here is easy to make and use, physical and chemical stable, continuous workable, and recyclable. The results show wide applications of the P25–graphene hydrogels in environmental protection issues.

4. Conclusions

In conclusion, we demonstrated the room-temperature synthesis of graphene-based hydrogels self-assembled from graphite oxide. Particularly, we found that the P25–graphene hydrogel could behave as a high performance photocatalyst, owing to its unique 3D structure and the chemical bonds between P25 and graphene. Furthermore, P25-hydrogels could be easily used as macroscopic environmental remediation devices with a strong adsorptivity. The maximum adsorption capacity of methylene blue to the hydrogel is obtained as much as 87.63 mg g^{-1}. The novel 3D TiO_2–graphene composite could be widely used in the environmental protection issues.

Acknowledgements

We gratefully acknowledge the financial support by Shanghai Municipal Education Commission (No. 07SG37), Natural Science Foundation of China (No. 51072034, 51172042), the Cultivation Fund of the Key Scientific and Technical Innovation Project (No. 708039), the Program for Professor of Special Appointment (Eastern Scholar) at Shanghai Institutions of Higher Learning, and the Program of Introducing Talents of Discipline to Universities (No. 111-2-04).

Appendix A. Supplementary data

Supplementary data associated with this article can be found, in the online version, at doi:10.1016/j.jhazmat.2011.12.071.

References

[1] K.S. Novoselov, A.K. Geim, S.V. Morozov, D. Jiang, Y. Zhang, S.V. Dubonos, I.V. Grigorieva, A.A. Firsov, Electric field effect in atomically thin carbon films, Science 306 (2004) 666–669.

[2] M.I. Katsnelson, Graphene: carbon in two dimensions, Mater. Today 10 (2007) 20–27.

[3] K. Yang, S. Zhang, G. Zhang, X. Sun, S.-T. Lee, Z. Liu, Graphene in mice: ultrahigh in vivo tumor uptake and efficient photothermal therapy, Nano Lett. 10 (2010) 3318–3323.

[4] C. Berger, Z. Song, X. Li, X. Wu, N. Brown, C. Naud, D. Mayou, T. Li, J. Hass, A.N. Marchenkov, E.H. Conrad, P.N. First, W.A. de Heer, Electronic confinement and coherence in patterned epitaxial graphene, Science 312 (2006) 1191–1196.

[5] Q. Wu, Y.X. Xu, Z.Y. Yao, A.R. Liu, G.Q. Shi, Supercapacitors based on flexible graphene/polyaniline nanofiber composite films, ACS Nano 4 (2010) 1963–1970.

[6] W.Y. Zhu, M.D. Stoller, W.W. Cai, A. Velamakanni, R.D. Piner, D. Chen, R.S. Ruoff, Exfoliation of graphite oxide in propylene carbonate and thermal reduction of the resulting graphene oxide platelets, ACS Nano 4 (2010) 1227–1233.

[7] Y. Zhang, Z.Q. Shi, Y. Huang, Y.F. Ma, C.Y. Wang, M.M. Chen, Y.S. Chen, Supercapacitor devices based on graphene materials, J. Phys. Chem. C 113 (2009) 13103–13107.

[8] Y.X. Xu, W.J. Hong, H. Bai, C. Li, G.Q. Shi, Strong and ductile poly(vinyl alcohol)/graphene oxide composite films with a layered structure, Carbon 47 (2009) 3538–3543.

[9] A. Cao, Z. Liu, S. Chu, M. Wu, Z. Ye, Z. Cai, Y. Chang, S. Wang, Q. Gong, Y. Liu, A facile one-step method to produce graphene-CdS quantum dot nanocomposites as promising optoelectronic materials, Adv. Mater. 22 (2010) 103–106.

[10] Z.P. Sun, T. Hasan, F. Torrisi, D. Popa, G. Privitera, F.Q. Wang, F. Bonaccorso, D.M. Basko, A.C. Ferrari, Graphene mode-locked ultrafast laser, ACS Nano 4 (2010) 803–810.

[11] J.C. Liu, H.W. Bai, Y.J. Wang, Z.Y. Liu, X.W. Zhang, D.D. Sun, Self-assembling TiO_2 nanorods on large graphene oxide sheets at a two-phase interface and their anti-recombination in photocatalytic applications, Adv. Funct. Mater. 20 (2010) 4175–4181.

[12] R.T. Lv, T.X. Cui, M.S. Jun, Q.A. Zhang, A.Y. Cao, D.S. Su, Z.J. Zhang, S.H. Yoon, J. Miyawaki, I. Mochida, F.Y. Kang, Open-ended, N-doped carbon nanotube-graphene hybrid nanostructures as high-performance catalyst support, Adv. Funct. Mater. 21 (2011) 999–1006.

[13] S. Park, R.S. Ruoff, Chemical methods for the production of graphenes, Nat. Nanotechnol. 4 (2009) 217–224.

[14] Y. Zhu, S. Murali, M.D. Stoller, W. Cai, P.J. Ferreira, A. Pirkle, R.M. Wallace, K.A. Cychosz, M. Thommes, D. Su, E.A. Stach, R.S. Ruoff, Carbon-based supercapacitors produced by activation of graphene, Science 332 (2011) 1537–1541.

[15] Z. Chen, W. Ren, L. Gao, B. Liu, S. Pei, H.-M. Cheng, Three-dimensional flexible and conductive interconnected graphene networks grown by chemical vapour deposition, Nat. Mater. 10 (2011) 424–428.

[16] Y. Xu, K. Sheng, C. Li, G. Shi, Self-assembled graphene hydrogel via a one-step hydrothermal process, ACS Nano 4 (2010) 4324–4330.

[17] X. Zhang, Z. Sui, S. Yue, Y. Luo, W. Zhan, B. Liu, Mechanically strong and highly conductive graphene aerogel and its use as electrodes for electrochemical power sources, J. Mater. Chem. 21 (2011) 6494–6497.

[18] Z. Sui, X. Zhang, Y. Lei, Y. Luo, Easy and green synthesis of reduced graphite oxide-based hydrogels, Carbon 49 (2011) 4314–4321.

[19] J.L. Vickery, A.J. Patil, S. Mann, Fabrication of graphene-polymer nanocomposites with higher-order three-dimensional architectures, Adv. Mater. 21 (2009) 2180–2184.

[20] F. Liu, S.S. Tae, A controllable self-assembly method for large-scale synthesis of graphene sponges and free-standing graphene films, Adv. Funct. Mater. 20 (2010) 1930–1936.

[21] Z.-J. Fan, W. Kai, J. Yan, T. Wei, L.-J. Zhi, J. Feng, Y.-M. Ren, L.-P. Song, F. Wei, Facile synthesis of graphene nanosheets via Fe reduction of exfoliated graphite oxide, ACS Nano 5 (2011) 191–198.

[22] T.N. Lambert, C.A. Chavez, B. Hernandez-Sanchez, P. Lu, N.S. Bell, A. Ambrosini, T. Friedman, T.J. Boyle, D.R. Wheeler, D.L. Huber, Synthesis and characterization of titania-graphene nanocomposites, J. Phys. Chem. C 113 (2009) 19812–19823.

[23] H. Zhang, X. Lv, Y. Li, Y. Wang, J. Li, P25-graphene composite as a high performance photocatalyst, ACS Nano 4 (2010) 380–386.

[24] Z. Tang, S. Shen, J. Zhuang, X. Wang, Noble-metal-promoted three-dimensional macroassembly of single-layered graphene oxide, Angew. Chem. Int. Ed. 49 (2010) 4603–4607.

[25] J. Du, X. Lai, N. Yang, J. Zhai, D. Kisaius, F. Su, D. Wang, L. Jiang, Hierarchically ordered macro-mesoporous TiO_2-graphene composite films: improved mass transfer, reduced charge recombination, and their enhanced photocatalytic activities, ACS Nano 5 (2011) 590–596.

[26] W.S. Hummers, R.E. Offeman, Preparation of graphitic oxide, J. Am. Chem. Soc. 80 (1958) 1339.

[27] G. Cao, Y. Li, Q. Zhang, H. Wang, Synthesis and characterization of $La_2O_3/TiO_{2-x}F_x$ and the visible light photocatalytic oxidation of 4-chlorophenol, J. Hazard. Mater. 178 (2010) 440–449.

[28] C. Nethravathi, M. Rajamathi, Chemically modified graphene sheets produced by the solvothermal reduction of colloidal dispersions of graphite oxide, Carbon 46 (2008) 1994–1998.

[29] S. Sakthive, H. Kisch, Daylight photocatalysis by carbon-modified titanium dioxide, Angew. Chem. Int. Ed. 42 (2003) 4908–4911.

[30] L.C.A. Oliveira, C.V.Z. Coura, I.R. Guimarães, M. Gonçalves, Removal of organic dyes using Cr-containing activated carbon prepared from leather waste, J. Hazard. Mater. 192 (2011) 1094–1099.

[31] J. Matos, A. García, L. Zhao, M.M. Titirici, Solvothermal carbon-doped TiO_2 photocatalyst for the enhanced methylene blue degradation under visible light, Appl. Catal. A-Gen. 390 (2010) 175–182.